Journal of Materials Chemistry A

REVIEW

View Article Online
View Journal | View Issue

Cite this: J. Mater. Chem. A, 2018, 6, 21847

Synergistic modulation in MX_2 (where M = Mo or W or V, and X = S or Se) for an enhanced hydrogen evolution reaction

Ran Wang,[a] Jiecai Han,[a] Xinghong Zhang*[a] and Bo Song *[ab]

Received 20th June 2018
Accepted 12th September 2018

DOI: 10.1039/c8ta05912h

rsc.li/materials-a

In order to solve the energy crisis and reduce the environmental impact of the combustion of fossil fuels, the strategy of obtaining hydrogen using the hydrogen evolution reaction (HER) has great potential. Being promising candidates for HER catalysts, two-dimensional (2D) layered transition metal dichalcogenides having the general formula MX_2 (where M represents Mo or W or V, and X denotes S or Se) have attracted significant attention. During the past several years, it has been found that synergistic effects were very important. According to some recent studies, reasonable synergistic modulation is beneficial for increasing the performance of the HER. In this work, the contribution of synergistic modulations in MX_2 materials towards the HER is investigated, and is expected to play a positive role in the development of high-efficiency catalytic materials.

1. Introduction

In the past few decades, hydrogen (H_2) has gained importance as a renewable clean energy resource, which can reduce both the consumption of fossil fuels and the resulting environmental issues.[1,2] At present, the large-scale production of hydrogen mainly relies on the pyrolysis of fossil fuels, which results in the consumption of large amounts of fossil fuels with the emission of significant amounts of greenhouse gas. For the efficient production of hydrogen in an environmentally friendly way, the hydrogen evolution reaction (HER) and the photoelectrochemical (PEC) splitting of water have become important strategies. Although platinum (Pt) and other precious metals have shown excellent catalytic activity for the HER in acidic media, their high cost and scarcity greatly limit their application on a large scale. Therefore, the development of novel and abundantly available electrocatalysts is needed, which could replace these rare and expensive precious-metal catalysts.[3–8]

In the past few years, significant research has taken place to explore such suitable electrocatalysts for the HER, which include transition metal sulphides,[9–14] selenides,[15–17] and phosphides.[18–20] Due to the success of graphene, enormous research enthusiasm exists regarding the potential of graphene-like two-dimensional (2D) layered materials.[21] Among these 2D materials, MX_2-type compounds (where M represents Mo or W or V, and X denotes S or Se) have received much attention, which is due to their unusual structural properties, unique crystal structures, and their promise for high HER performance.[22–24] Due to their similarity to graphene-like 2D structures, many routes used for the synthesis of graphene are also effective for preparing MX_2 nanosheets (NSs), which helps in further boosting the rapid development in this field. Both theoretical and experimental efforts have contributed to overcoming the intrinsic shortcomings of bulk MX_2 materials, and include optimizing the synthesis methods, tuning the crystal structures, and thoroughly understanding the mechanism of their catalytic performance.[25–29]

In order to further enhance the HER performance of MX_2-based materials, researchers have put forward a series of strategies, including phase engineering, electronic engineering, defect engineering or interlayer engineering, which have achieved significant progress in developing MX_2 for high HER performance.[30–33] For example, phase engineering could enhance the internal electrical conductivity of MX_2 from

[a]Centre for Composite Materials and Structures, Harbin Institute of Technology, Harbin 150001, China. E-mail: zhangxh@hit.edu.cn
[b]Academy of Fundamental and Interdisciplinary Sciences, Department of Physics, Harbin Institute of Technology, Harbin 150001, China. E-mail: songbo@hit.edu.cn

Prof. Bo Song is a full professor of Physics in Harbin Institute of Technology. He received his Ph.D. from the Institute of Physics (2008), Chinese Academy of Sciences (CAS). His current research focuses on electrochemical energy storage devices, two-dimensional materials and semiconductor optoelectronic devices.

a semiconducting 2H phase to a metallic 1T-phase crystal structure, which shortens the migration resistance between the electrons and the active sites and boosts the HER activity.[34] Similarly, electronic engineering could modulate the band-gap of the MX_2 inert basal plane, which provides higher electrical conductivity, and lowers the barrier for kinetic energy.[35] Moreover, defect engineering could result in the partial cracking of the catalytically inert basal-plane, which leads to the exposure of more active edge sites involved in catalytic activity.[30] Meanwhile, interlayer engineering was used to effectively expand the interlayer spacing, which increases the abundance of exposed active sites.[36] Although the above strategies significantly enhanced catalytic activity towards the HER, it is still a challenge to rival Pt or other noble metals by tuning a single factor.[37] After a thorough understanding of these factors, pursuing synergistic modulation to effectively maximize their advantages could further enhance the catalytic activity of MX_2-based electrocatalysts during the HER.

In addition to the synergistic regulation of internal factors in MX_2 catalysts, they can also be combined with other functional materials, including conductive media, heterogeneous components and electronically coupled interfaces, to combine the advantages of both the materials,[38] and perform according to the principle of "two are better than one".[39] Conductive media, such as graphene, carbon fibres, and their derivatives, have large surface areas and excellent electrical conductivities, and have been used for synthesizing composites using MoX_2 NSs.[40] Through the synergistic modulation of each component, composite catalysts that are integrated with abundant catalytically active sites and high electron transportation achieve excellent HER performance as MX_2 materials. Furthermore, the synergistic hybrid catalyst, having a heterogeneous structure, could benefit from the advantages of each component and the higher interfacial area. Synergistic heterogeneous structures of various materials not only make multi-functional catalysts challenging for the overall water splitting process, but also solve the bottleneck of using MX_2 in alkaline media, and help develop high-activity MoX_2-based electrocatalysts for comprehensive pH media.[41]

Although the catalytic activities of MoX_2-based catalysts have been significantly boosted over the last few decades,[42–44] the integration of robust catalyst design strategies is urgently needed, which selectively enhance the performance indicators of these catalysts. The synergistic mechanisms could offer valuable understanding for the further design of catalysts and open up opportunities to develop high-performance electrocatalysts for a wide range of reactions. This review focuses on the contribution of the synergistic modulation of MX_2 materials towards the HER and divides it into four parts. Based upon theoretical proofs and experimental results regarding different electrochemical reactions, the optimization mechanism in the HER is clarified, which serves as a guide for the development of new catalysts and discussion of the key gaps in MX_2-based catalysts. It is expected that the results will help in the development of improved catalysts, which could allow for efficient production of clean energy carriers, such as hydrogen.

2. Coordinate internal factors

Due to the poor conductivity of the semiconducting 2H phase, it is difficult for free electrons to transfer between the electrode and active site, making them inferior to noble metal-based electrocatalysts. Phase engineering from the semiconducting 2H phase to the metastable metallic 1T-phase MX_2 has been demonstrated as an effective strategy to improve the catalytic activity of these materials.[31] In view of this, other favourable factors are also introduced in the 1T-phase crystal structure for guaranteeing high electrical conductivity, which can help achieve more catalytically active sites. As a typical example, Song and co-workers prepared a series of partially crystallized 1T-phase $MoSe_2$ NSs using excess $NaBH_4$ precursor through the hydrothermal-synthesis strategy.[36] Based upon the characterization of structures and properties, it was found that the catalytic performance during the HER could be enhanced using the synergistic regulation of the crystal phase and disorder. Positron annihilation lifetime spectroscopy (PALS) was used to characterize the defects, induced by the lower temperature of the hydrothermal reaction, which could provide abundant active sites. After applying electrochemically active surface area (ECSA) characterization to the electrocatalysts, the double-layer capacitance (C_{dl}) for the representative sample was obtained to be 27.8 mF cm^{-2}. These results suggest that the degree of disorder in 1T-phase $MoSe_2$ materials can be effectively controlled by simply tuning the synthesis temperature. The synergistic effects successfully boost the catalytic activity for the HER with an overpotential of 152 mV at a current density of -10 mA cm^{-2} and a Tafel slope of 52 mV dec^{-1}. In addition, Song and co-workers prepared porous metallic 1T-phase MoS_2 NSs using a liquid ammonia-assisted lithiation method, and the contributions of crystal structures (phase), edges, and S vacancies to the catalytic activity towards the HER were systematically investigated (Fig. 1a–b).[45] The ECSA between the porous 2H phase MoS_2 and the corresponding sample was comparatively reduced with sulphur compensation, which is an indication that the S-vacancies may promote the HER activity by providing more active sites. Due to the synergistic effects of the metallic phase and active sites, superior HER catalytic performance was achieved in the porous 1T-phase MoS_2 NSs, as compared with the single regulation (Fig. 1c). Moreover, Zhang and co-workers reported a common and simple strategy involving combining the ball-milling and lithium-intercalation methods, which could efficiently synthesize single-layered transition metal dichalcogenides (TMDs) having high-density active edge sites and high-proportion 1T-phase content (Fig. 1d).[46] Herein, the as-synthesized 1T-phase MoS_2, $MoSe_2$, MoSSe, WS_2, and $Mo_{0.5}W_{0.5}S_2$ nanodots (ND) revealed higher HER performances, compared with the corresponding 1T-phase NS samples. Among these TMD samples, MoSSe ND exhibited satisfactory results, with an overpotential of 140 mV at a current density of -10 mA cm^{-2} and a Tafel slope of 40 mV dec^{-1}. In addition, they also showed good long-term durability (Fig. 1e). Due to the combining of high-density active edge sites with the selenium-vacancy of the basal-plane, a high-proportion metallic

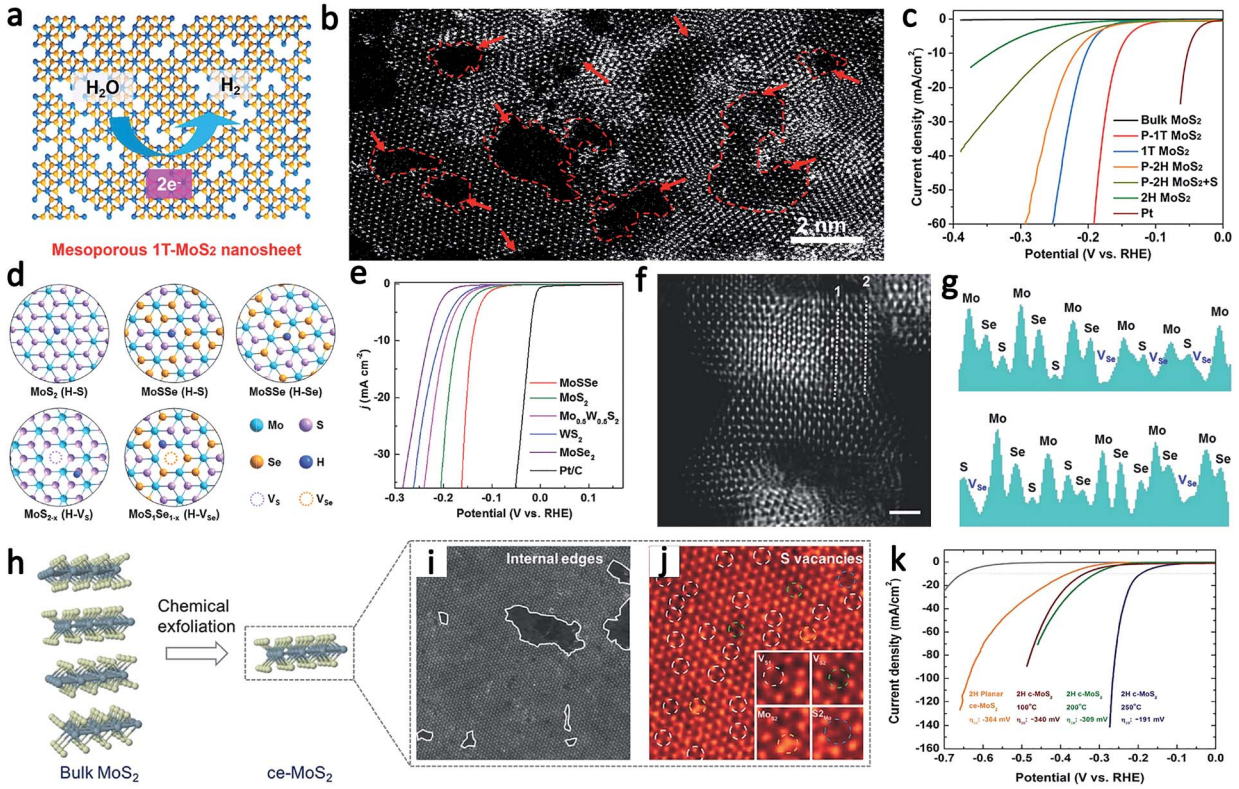

Fig. 1 (a) Schematic of the mesoporous 1T phase MoS_2 NSs (P-1T-MoS_2), (c) J–V curves after the iR correction of various MoS_2 samples in comparison to a Pt wire, and (b) the high-resolution STEM image of P-1T-MoS_2 NSs. Copyright 2016, American Chemical Society.[45] (d) Atomic models for hydrogen atoms adsorbing at the active sites of basal planes; V_S and V_{Se} represent S and Se vacancies, respectively, (e) the electrochemical HER performance of MoSSe nanodots, (f) The L2D-WF ABSF filtered image of MoSSe nanodots, and (g) Brightness profiles along the dotted lines in (f). Copyright 2018, Wiley.[46] (h) The chemical exfoliation process of bulk MoS_2 powder, (i) the TEM image, (j) HAADF image, and (k) A series of MoS_2-based HER characteristics. Copyright 2017, Wiley.[42]

1T-phase is obtained, whose characterization of structure and properties suggests that the catalytic performances of MoSSe ND are excellent (Fig. 1f–g).

Although, compared to the semiconducting 2H-phase, the metallic 1T-phase exhibits good intrinsic conductivity, the metastable state of the 1T-phase is easy to metamorphose, which limits its further application and production.[34,47,48] In order to overcome this obstacle, incorporation of the electronic structure with controllable exposed active sites may equal the effect of the synergistic modulation of both the conductivity and the active sites towards the HER. For example, Xie and co-workers reported that both the oxygen incorporation and the disorder engineering in MoS_2 NSs could be beneficial to the synergistic regulation of electronic structures, which results in dramatically improved HER performance.[49] Furthermore, density-of-states (DOS) calculations demonstrated that the band gap of the oxygen-incorporated MoS_2 plane is 1.30 eV, which is narrower than that of the primitive MoS_2 plane, and could have more charge carriers and higher intrinsic electrical conductivity, due to which the controllable electronic modulation was realized. The incorporation of oxygen is capable of actually optimizing the electronic structure while the disordered crystal structure is able to provide plentiful V_S as catalytic sites for the HER. In addition, Xie and co-workers presented a one-step hydrothermal method to accomplish defect engineering in ultrathin MoS_2 NSs.[30] The satisfactory electrocatalytic performance of the defect-rich ultrathin MoS_2 NSs is attributed to the synergistic effect of enriched active edge sites caused by abundant defects and the ultrathin NS structure. In ultrathin NSs, the existence of rich defects would change the catalytically inert basal plane to partial cracking, which results in the exposure of more active edge sites. The defect-rich MoS_2 ultrathin NSs possess the highest density of active sites with a value of 1.785×10^{-3} mol g^{-1}, which is 2.9 times higher than that of the defect-free NSs and 13 times higher than that of bulk MoS_2. Such a high density of active sites provides direct evidence of the predominant enrichment effect of active edge sites brought by the rich defects. Modulating the interlayer distance would be a potential method to design novel and efficient MX_2 catalysts to improve electrochemical performance.[50] Sun and co-workers prepared narrow nanostructured MoS_2 NSs using a promising microwave-assisted method, which were equipped with edge-terminated construction and an effective interlayer-expanded space.[51] The edge-terminated construction provides more active edge sites, whereas the interlayer-expanded distance can regulate the electronic structure, which gives a large C_{dl} of 15.3 mF cm^{-2} and a current density of -10 mA cm^{-2} at an overpotential of 0.149 V. Due to the synergetic coupling effects of both the terminated edge and expanded interlayer, the MoS_2 NSs had the smallest charge transfer resistance (R_{ct}) of only

3.13 Ω, which provides an insight into the electrode kinetics during the HER process. Similarly, Lu and co-workers designed an interlayer-expanded layered VS_2 using a one-pot solvothermal strategy with expanded interlayer space and rich defects.[52] The interlayer spacing had a significant 74% increase from 0.575 nm to 1.00 nm, which increased the number of exposed active sites, and resulted in a much larger C_{dl} value of 151 mF cm^{-2}. Meanwhile, the defect-rich VS_2 NSs with an enlarged interlayer space resulted in a free energy of hydrogen adsorption (ΔG_H) value of −0.044 eV, which was computed using the density functional theory (DFT). The synergistic modulation of interlayer expansion and defect engineering in VS_2 NSs exhibited extraordinary HER performance, with a small Tafel slope of 36 mV dec^{-1} and a low overpotential of 43 mV at a current density of −10 mA cm^{-2}, which are close to those of the Pt/C system. Generally, creating more active sites on MoS_2 through an exfoliation strategy could create more exposed edges. Ye and co-workers synthesized single-deck enriched MoS_2 NSs using a flexible compound centrifugation-assisted liquid exfoliation strategy to promote photocatalytic hydrogen generation using MoS_2.[53] Due to the synergetic effect of liquid phase exfoliation and lateral size selection engineering, more exposed active sites at the edge were obtained and the migration distance between the electrons and the active sites was shortened. The catalytic performances of MoS_2 monolayers could be dramatically improved in both electrocatalytic and photocatalytic hydrogen evolution with nanoscale lateral sizes continuously decreasing from 42 to 9 nm. In particular, the MoS_2 monolayers with a lateral size of 9 nm could result in a catalytic current density of −10 mA cm^{-2} at an overpotential of 192 mV. Although, comparable to commercial Pt/C catalysts, many MX_2-based materials having excellent catalytic performance have been reported, the balance between the catalytic activity and the long-term stability still represented an inevitable challenge. Tung and co-workers reported a metastable and temperature-sensitive chemical exfoliation method for effectively synthesizing MoS_2 with structurally deformed nanostructures, which could be electrochemically stable and have excellent catalytic activity (Fig. 1h).[42] A high-productivity electrohydrodynamic (EHD) process, which is a deposition method with a high electric field, combined with the chemical exfoliation, can introduce internal edges and V_S on the basal plane, thus affording electrochemically active plane sites and enhancing the efficient transport between various interfaces (Fig. 1i–j). The number of active sites was estimated using the underpotential deposition (UPD) method, and the density of active sites was determined to be around 1×10^{14} sites per cm^2 for the 2H-phase chemically exfoliated MoS_2. The density of active sites further increased to 5.86×10^{17} sites per cm^2 for the 2H-phase crumpled MoS_2. Furthermore, the hierarchically strained structure can synergistically facilitate the electronic combination between the active sites and current collecting substrates (Fig. 1k).

3. Optimizing the basal plane

The HER is a complex electrochemical process, and includes energy conversion and interfacial behaviour.[54] Therefore, new strategies for material design are required to exploit the potential of MX_2 and optimize each pivotal step during the reaction. As the recognized active site of catalytic activity, the edge of MX_2 is precious and limited.[43] Due to the inertia of the basal plane, the catalytic activity of MX_2 cannot be exploited effectively and favourably. Although it has also been suggested that basal plane sites of 1T-MoX_2 NSs are active catalytic sites, their positive effect on HER performance is limited as compared to that of the edge sites.[55] Therefore, by introducing synergistic effects to the basal plane, the electrocatalytic performance of MX_2 can be greatly improved. The strategy of single-atom doping has been widely used in the synthesis of electrocatalysts. Heteroatom-doped graphene[56,57] is able to significantly modulate the catalytic activity in-plane, suggesting that the heteroatom-doping strategy could also be applied to 2D MoX_2. It can trigger the hydrogen evolution activity of sulphur atoms in the inert plane of MoS_2.[58] For instance, Bao and co-workers reported a multiscale structure of MoS_2 foam with uniform mesopores, vertically aligned layers and doped cobalt atoms, which synergistically boosted the hydrogen evolution process due to electronic control through a direct chemical synthesis method.[59] When doping another metal atom into MoS_2 in-plane, the electron number on the S atom will decrease to offset the mismatching of the energy level, thus enhancing the H adsorption and HER activity. Among them, the Co atom is indeed a good regulator to bring ΔG_H to approximately 0 eV. Moreover, the influence of different Co content within the basal plane of MoS_2 on the HER activity was well understood according to the DFT calculations and experimental results. Therefore, hybridizing transition metal atoms with mesoporous MoS_2 foam using atomic-scale doping engineering can synergistically promote the performance of the HER. For the selection of precious metals for the edge and terrace surface in WS_2, Yan and co-workers demonstrated that the 2D WS_2 NSs with rich exposed edges will display a much stronger interaction with Pt atoms, which is due to the terminal S_2^{2-} or S^{2-} ligands on the edge exhibiting much lower binding energy for Pt atoms, as compared to the apical S^{2-} ligands on the terrace surface.[60] These results indicated that the edge sites are active for Pt deposition, while the basal plane is inert. Moreover, Cui and co-workers showed the heterostructure between a Pd nanodisk (Pd-ND) and defect-rich MoS_2 (DR-MoS_2) NSs, with the synergistic regulation of both the structure and electronic states, which exhibited outstanding HER properties.[61] The heterostructure was realized by synthesizing and constructing a disk-like Pd nanostructure on the basal plane of DR-MoS_2. Based upon theoretical calculations and experimental characterizations, the basal plane of DR-MoS_2 with adsorbed Pd atoms could effectively regulate the surface electronic state of MoS_2, while simultaneously retaining its active sites, which greatly improved the HER activity. Furthermore, Chen and co-workers reported a strategy which involved engineering the energy level of MoS_2 by directly doping the transition metal to enhance its HER performance (Fig. 2a–b).[62] The excellent electrochemical activity of zinc doped MoS_2 (Zn–MoS_2), synthesized using a modified hydrothermal method, can be attributed to the synergistic effect of the electronic effect of matching energy

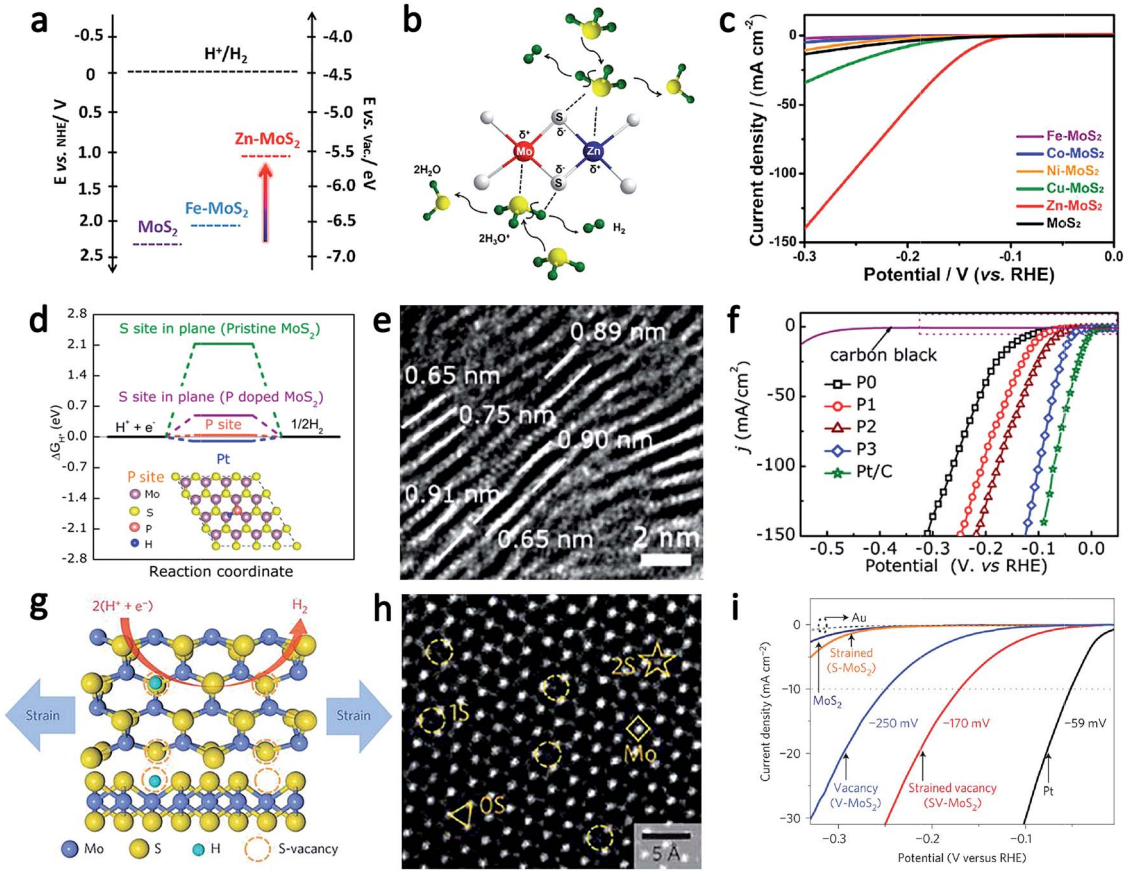

Fig. 2 (a) Band structure diagram for Zn–MoS_2, Fe–MoS_2, and pure MoS_2, (b) Schematic of the formation of undercoordinated Mo (δ^+) and Zn (δ^+) centres during the HER and the plausible reaction mechanism, (c) the electrochemical activities of various X–MoS_2 (x = Fe, Co, Ni, Cu, and Zn) catalysts towards the HER. Copyright 2017, American Chemical Society.[62] (d) The HER free-energy diagram for P and S sites in the basal plane of pristine and P-doped MoS_2, (e) the stand-up edges for P-doped MoS_2 NSs, and (f) the polarization curves of pure and P-doped MoS_2 NSs in 0.5 M H_2SO_4. Copyright 2017, American Chemical Society.[67] (g) Schematic of the top and side views of MoS_2 with strained S-vacancies on the basal plane, where S-vacancies serve as the active sites for hydrogen evolution and applied strain further tunes the HER activity, (h) the ACTEM image of a MoS_2 monolayer, and (i) the LSV curves for the Au substrate, Pt electrode, and as-prepared MoS_2. Copyright 2015, Nature Publishing Group.[32]

levels and the rich active sites through thermodynamic and kinetic acceleration (Fig. 2c). As the energy level increases, the energy required to remove an electron from the catalyst surface will decrease, which thermodynamically activates the HER. Ultraviolet photoelectron spectroscopy (UPS) of transition metal doped MoS_2 depicts that, compared to the reduction potential of H_2O, the energy level of Zn–MoS_2 is properly positioned to permit electron transfer with much lower applied energy, thus confirming that Zn–MoS_2 is a promising electrocatalyst for the HER. Guo and co-workers reported that heterogeneous spin states could achieve synergistically regulated active sites and dynamics in MS_2 catalysts, which boosts the performance of the HER.[63] The subtle distortion of atom arrangement would be able to synergistically provide additional active edge sites for the HER because Mn atoms were incorporated into the primitive lattice of $CoSe_2$ atomic layers. DFT calculations showed that the incorporation of Mn atoms could promote the formation of H–H bonds between the adsorbed adjacent H atoms to decrease the barrier of kinetic energy, which will efficiently promote the HER process. Ye and co-workers reported an extraordinary design of 2H-phase MoS_2 monolayers, involving the substitution of a Co atom and combining crystallinity engineering, which maximized the synergistic effect for HER activity.[64] Beyond the new active sites introduced by massive defects, the inert basal plane of the MoS_2 nanostructure was reactivated due to the synergistic regulation of Co doping and crystallinity engineering. Moreover, electrochemical measurements and DFT calculations demonstrated that the much enhanced HER activity is caused by the synergistic effect, as compared to individual Co substitution or crystallinity engineering. In addition, some divalent transition element ions can further promote the activity of catalysts. Hu and co-workers synthesized amorphous MoS_{2+x} using electrodeposition or a wet-chemical process.[12] The results indicated that divalent Fe, Co, and Ni ions can boost the growth of the MoS_{2+x} film, thus adjusting the layer thickness, catalyst loading, structural porosity, and active surface area.

Besides metal doping, doping non-metals can also improve the electrocatalytic properties for the HER, and this is achieved through the synergies of two or more items of the basal plane,

edge sites, inherent conductivity, and interlayer spacing. Recently, Wang and co-workers demonstrated effective boron doping-induced activation of both the basal plane and Se-edge in vertically grown $MoSe_2$ NSs, which was verified using both theoretical calculations and experiments, and can disruptively enhance the catalytic activity for the HER.[65] B doping greatly promoted the electrocatalytic activity of $MoSe_2$ for the HER, with a low overpotential of 84 mV at a current density of −10 mA cm^{-2} and Tafel slope of 39 mV dec^{-1}. The computational study revealed that B dopants induced strong hybridizations among Mo 3d, S 2p and B 2p orbitals, which led to the emergence of a narrowed band gap and increased electrical conductivity in $MoSe_2$, which in turn facilitated electron movement and charge transfer. Moreover, the ΔG_H value for the B sites in $MoSe_2$ was reduced to −0.05 eV due to the doping of B atoms, which is very close to that of Pt, suggesting that B dopants became the new active sites in the basal plane of the B-doped $MoSe_2$ electrode. According to experimental results, the C_{dl} value of B–$MoSe_2$ was 21 mF cm^{-2}, which is five times higher than that of $MoSe_2$, and indicates the effectiveness of electrochemical surface areas brought by the doping of non-metals. Furthermore, Ding and co-workers achieved an efficient MoS_2-based HER catalyst by doping nitrogen in the edges and basal plane of MoS_2 NSs, which resulted in an overpotential of 121 mV at −100 mA cm^{-2} and a Tafel slope of 41 mV dec^{-1}.[66] The N dopants not only activated the catalytically active sites for the HER, but also benefited rapid charge transfer, thus improving the electrical conductivity of the MoS_2 basal plane. This is due to the strong Mo 3d–S 2p–N 2p hybridizations at the Fermi level. The synergistically activated regulations of the basal plane and the edge sites of S and Mo favour the adsorption energies of hydrogen, which improves the electrocatalytic performance. Similarly, based upon calculations and experiments, Xue and co-workers reported a class of P dopants in the basal plane of MoS_2 as new active sites for electrocatalysis, which improve the intrinsic electronic conductivity and could result in a significant enhancement of the HER (Fig. 2d).[67] In addition, the P-doped MoS_2 NSs exhibited enlarged interlayer spacing (Fig. 2e), which can facilitate the progress of adsorption and release of hydrogen with a low overpotential of 43 mV at −10 mA cm^{-2} and Tafel slope of 34 mV dec^{-1} (Fig. 2f). Except for the exposed interlayer spacing, P-doping could also dramatically decrease the Mo valence charge, which leads to the activation of the inert MoS_2 basal plane and S-edge for the improvement of catalytic activity for the HER.[68,69]

Although activating the MoS_2 basal plane using element doping could enhance its catalytic HER performance, alternative strategies that fully utilize the 2D flexible properties of MoS_2 to activate the basal plane are still required.[70] Zheng and co-workers reported an alternative PMMA-assisted wet transfer method for activating the basal plane of the monolayer 2H-phase MoS_2 by introducing strain and V_S (Fig. 2g–h).[32] The experimental and computational results indicated that the V_S in the basal plane could regulate the Fermi level and provide new catalytic sites. Meanwhile, the strain in the basal plane with V_S would be able to optimize the free energy (ΔG_H) for the adsorption of hydrogen, generating an optimum value close to 0 eV, which could achieve outstanding HER activity (Fig. 2i). Moreover, the thermodynamically stable and naturally present defects could provide the basal plane of 2H-phase transition metal chalcogenides with high electrochemical activity, as compared to the metallic 1T-phase polymorph.[71]

4. Promoting electron transport

In order to overcome the limited number of active sites and poor semiconductor conductivity of 2H-phase MX_2, conductive substrates with large specific surface area and significantly high electron transfer capacity were used as composites, thus enhancing the catalytic activity. Graphene,[72] carbon fibres,[73,74] black phosphorus (BP),[75] nickel bases,[76] and their derivatives[77,78] have been widely used for preparing composites with MX_2 NSs. For example, Dai and co-workers developed an optional solvothermal synthesis of MoS_2 nanoparticles (NPs) on reduced graphene oxide (RGO) sheets dispersed in solution (Fig. 3a).[79] The small size and high charge number of MoS_2 NPs on RGO afforded a lot of active edges, which served as active catalytic sites for the HER. Meanwhile, an interconnected conducting network afforded the electrical coupling to underlying graphene sheets, and ensured rapid electron transport between MoS_2 NPs and electrodes. The MoS_2/RGO hybrid exhibited much lower impedance than free MoS_2 particles. With highly exposed edges and excellent electrical coupling with underlying graphene sheets, the MoS_2/RGO hybrid catalyst exhibited excellent HER activity with small overpotential, large cathodic currents, and

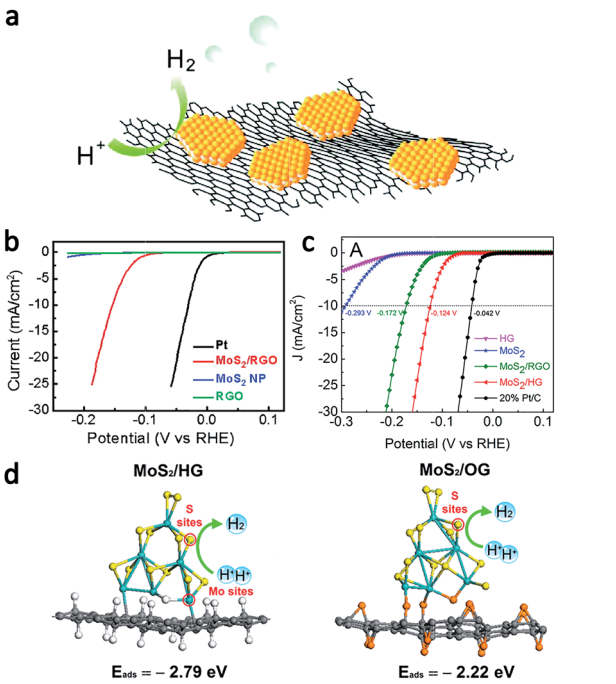

Fig. 3 (a) Synthesis of MoS_2 in solution with graphene sheets, (b) Polarization curves obtained with several MoS_2/RGO catalysts. Copyright 2011, American Chemical Society.[79] (c) Linear sweep voltammograms of a series of MoS_2/HG catalysts, (d) the optimized electronic structure of MoS_2 on HG, and on OG. Copyright 2018, American Chemical Society.[80]

a Tafel slope as small as 41 mV dec^{-1} (Fig. 3b). Similarly, Guo and co-workers introduced hydrogenated graphene (HG) sheets into MoS_2 NSs, which resulted in highly efficient and stable electrocatalysis for the HER (Fig. 3c).[80] After applying DFT calculations to MoS_2/HG compound catalysts, the H_{ads} (hydrogen adsorption) energy for MoS_2 on HG was calculated to be −2.79 eV, which is comparable to that of MoS_2 on oxidized graphene (OG), and is closer to that for Pt (−3.3 eV) (Fig. 3d).[58] Due to the synergistic effect between electronic and structural benefits of MoS_2 NSs due to the HG compound, such a strategy effectively optimizes the electronic structure, generates additional Mo active sites from C–Mo bonds, and optimizes the adsorption energy of hydrogen. Moreover, Guo and co-workers successfully synthesized MoS_2 NSs on selectively promoted graphene using a heterogeneous nucleation/growth strategy, and the results showed that the active edge was exposed and the interlayer spacing expanded the MoS_2 NSs grown on RGO NSs, thus resulting in a larger current density and lower Tafel slope.[81] The interlayer spacing of MoS_2 NSs was successfully expanded to 9.4 Å, due to the advantage of excellent heterogeneous nucleation and special reaction kinetics in the microwave solvothermal reaction. It is very advantageous to construct MoS_2 nanostructures, which can synergistically regulate both the high-density active edges and the expanded interlayer spacing, as they could significantly improve the HER catalytic activity of MoS_2. In addition, Banerjee and co-workers reported a stepwise synthesis strategy, which enhanced the electrocatalytic properties of MoS_2 NSs integrated onto carbon fibre paper (CFP) substrates and was achieved by interfacing with solution deposited buckminsterfullerene (nC_{60}).[82] The p–n heterojunctions between nC_{60} and MoS_2 constructed the interfacial layer, which promoted the charge transfer from nC_{60} nanoclusters to MoS_2 NSs and mitigated the limitations of the inert basal plane conductivity of pure MoS_2. This result indicated that the synergistic effect between the inherent catalytic active edge sites of MoS_2 NSs and the hybridization introduced by nC_{60} can enhance the electrocatalytic activity for the HER. Similarly, Cui and co-workers constructed MoS_2 NPs on carbon fibres following lithium electrochemical intercalation, and achieved an outstanding HER performance with −200 mA cm^{-2} cathodic current density at only 200 mV overpotential and excellent electrochemical stability.[83] The excellent catalytic activity profited from the metallic 1T-phase converted through the 2H semiconducting phase of MoS_2 and the largely exposed edge sites on the 3D carbon fibres with high surface area. In addition, Li and co-workers developed a facile hydrothermal method to vertically grow ultrathin MoS_2 NSs on the surfaces of carbon fibre cloths.[84] After the NH_4F etching effect, the number of active edge sites of MoS_2 can be significantly increased. Meanwhile, electrons can rapidly be transferred from the highly conductive carbon fibre cloth to the active edges of the MoS_2 NSs, which considerably enhanced the electrical conductivity of MoS_2 NSs. The synergistic effect between the number of active edge sites and the conductivity led to the superior activity of MoS_2 composites toward the HER.

The successful exploration of graphene has recently inspired great research enthusiasm regarding 2D layered materials. As a typical representative, layered BP has attracted enormous attention due to its high mobility.[85,86] Zeng and co-workers reported the catalytic activity of MoS_2 NSs deposited on BP with engineered electronic properties.[87] Typically, MoS_2-BP NSs were synthesized by sonicating precursors of MoS_2 and BP in ethanol, followed by a solvothermal treatment. The flat-band potential (U_F) of BP NSs was about −0.29 V, which was more negative than that of MoS_2 flakes. Due to the reason that U_F can denote the Fermi level (E_F) position with respect to the electrochemical potential of the redox couple in the electrolyte, the E_F of BP was higher than that of MoS_2 flakes. As a result of the E_F equilibrium, electrons could transfer from BP to MoS_2 in MoS_2-BP NSs.[88] In particular, MoS_2-BP NSs exhibited outstanding electrocatalytic stability and excellent kinetics with an overpotential of 85 mV at −10 mA cm^{-2}. In addition, Li and co-workers reported 3D nickel foam (NF), which had graphene layers grown on its surface, and was used as a conductive carrier support to synergize MoS_x catalysts for electrocatalytic hydrogen evolution.[89] The graphene NSs deposited on NF provided adequate protection and efficiently promoted its stability in acid.[90] Because of the rough surface of the deposited MoS_x NSs and the special structure of 3D graphene/NF, large amounts of edges provided more catalytically active sites. The advantage of employing 3D NF as an electrode is not only the provision of a large surface area and superior conductivity, but also the loading weight of the MoS_x catalyst, which is larger than those of other carbon-based electrodes, and thus leads to the enhancement in HER efficiency.

Furthermore, as a promising method to provide hydrogen for a clean and reproducible energy carrier, solar-driven photoelectrochemical (PEC) water electrolysis is also of great importance. For example, Jin and co-workers synthesized a high-activity amorphous MoS_xCl_y HER electrocatalyst using a low-temperature chemical vapour deposition (CVD) method.[91] Compared with other MoS_2-like electrocatalysts, the high catalytic performance of MoS_xCl_y deposited on conducting vertical graphene for the HER is attributed to the synergistic effect of high electrochemical activity and large electroconductive surface area. In addition, this MoS_xCl_y electrocatalyst can also be deposited on a Si micro-pyramid (MP) to form an integrated photocathode, which synergistically regulates the high transparency of MoS_xCl_y and results in the efficient light-trapping performance of the Si MP structure, thus ensuring efficient solar-driven photoelectrochemical hydrogen production.[92,93]

5. Constructing the heterogeneous interface

The composition and structure of hybrid materials mainly determine their electronic, photoelectric and chemical properties.[94,95] Therefore, the construction of heterogeneous structures is critically important for improving the performance of non-precious metal catalysts. For example, Yu and co-workers reported a stable and efficient HER-catalyst which is synthesized by the *in situ* synthesis of MoS_2 on the surface of $CoSe_2$ (Fig. 4a).[96] The MoS_2/$CoSe_2$ catalyst showed excellent HER

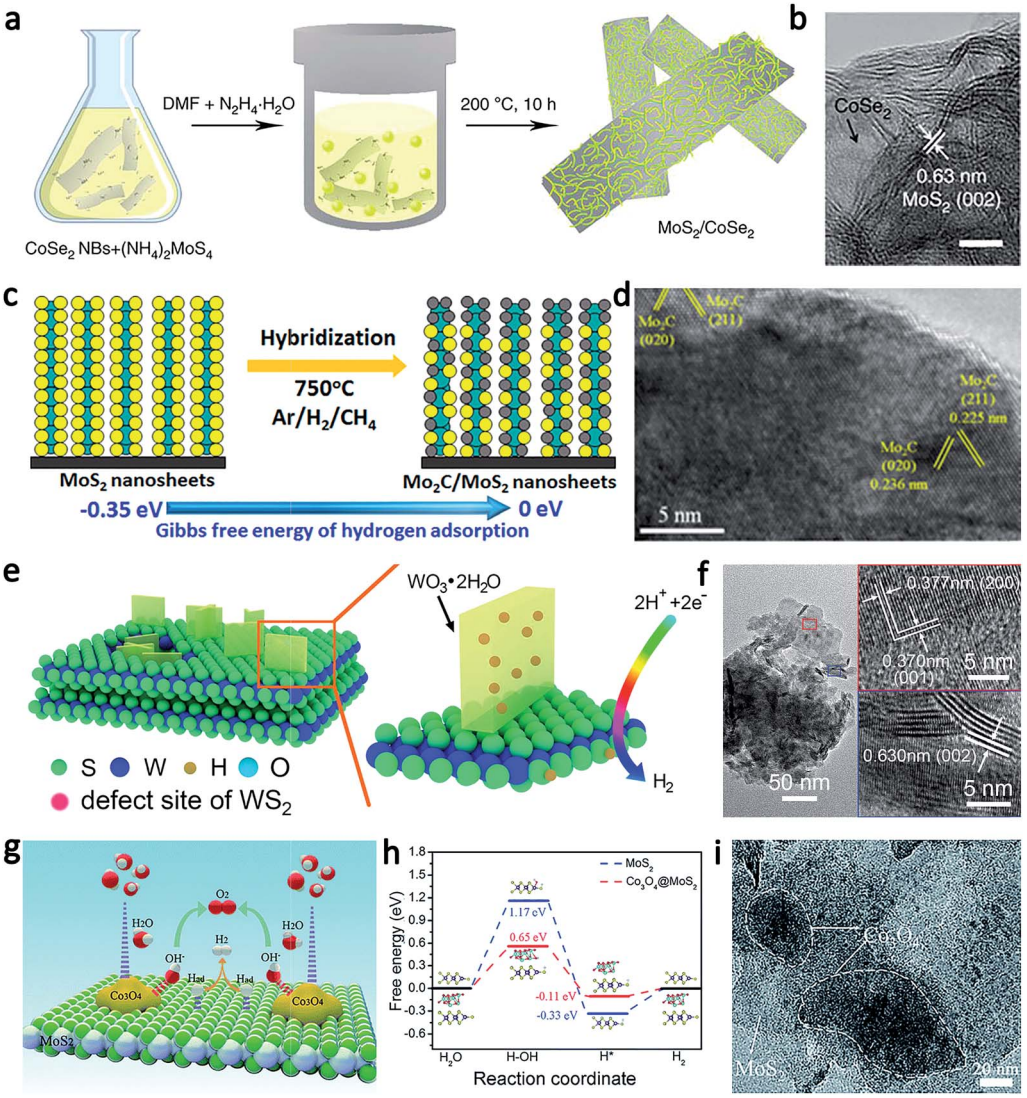

Fig. 4 (a) Schematic of the preparation of $MoS_2/CoSe_2$ hybrids, and (b) HRTEM images of the $MoS_2/CoSe_2$ hybrid showing distinguishable microstructures of MoS_2 and $CoSe_2$. Copyright 2015, Nature Publishing Group.[96] (c) A schematic of the steps for the synthesis of vertically aligned MoS_2/Mo_2C hybrid NSs, and (d) the HRTEM image of the MoS_2/Mo_2C hybrid NSs. Copyright 2017, American Chemical Society.[96] (e) A schematic of the structure of $WO_3 \cdot 2H_2O$ nanoplates on a WS_2 film after anodic treatment, and (f) the TEM image of WS_2. The red- and blue-framed insets correspond to $WO_3 \cdot 2H_2O$ and WS_2 regions, respectively. Copyright 2016, American Chemical Society.[101] (g) A schematic of the HER and OER processes on Co_3O_4@MoS_2 interface structures, (h) the free energy diagram for the HER on the MoS_2 edge and Co_3O_4@MoS_2 heterostructure catalyst, and (i) the TEM image of Co_3O_4@MoS_2/CC. Copyright 2018, Royal Society of Chemistry.[110]

kinetics with an overpotential of 68 mV at a current density of -10 mA cm^{-2} and a Tafel slope of 36 mV dec^{-1}. Due to the synergistic effects between the MoS_2 and $CoSe_2$ hybrid catalyst, more active edge sites may be enriched by amorphous MoS_2 around $CoSe_2$, which can further enhance the HER activity (Fig. 4b). Zhang and co-workers described a special Co_9S_8@MoS_2 core–shell structure on carbon nanofibers (CNFs), where the core was cubic Co_9S_8 and the shell was layered MoS_2.[97] Both the HER and OER electrocatalytic performances of the unique Co_9S_8@MoS_2/CNFs hybrid catalyst were substantially enhanced by combining the functions of MoS_2 and Co_9S_8 with the synergetic effects of the interface between the Co_9S_8 core and the MoS_2 shell. Electron transfer takes place where the localized interface area between MoS_2 and Co_9S_8 exists, and results in promoting the electrocatalytic activity. Bao and co-workers reported a vertically aligned MoS_2/Mo_2C hybrid nanostructure on conductive carbon paper (Fig. 4c).[98] After the carburization of MoS_2 NSs, the vertical nanostructure of MoS_2 remained with the Mo_2C edges and the heteroatomic mixture between S and C. In the synergistic integration structure, high conductivity benefited from Mo_2C nanocrystals, whereas the large number of edge sites profited from the 2D MoS_2 NSs. Compared with the homologous Mo_2C and MoS_2, the MoS_2/Mo_2C catalyst provided a lower overpotential during the HER. The Gibbs free energy of hydrogen adsorption is close to zero due to active S and C synergetic Mo sites, which is well consistent with the results obtained from the DFT calculations. Therefore, the low overpotential of the MoS_2/Mo_2C catalyst was attributed to the active

sites of synergistic regulation and uniformly dispersed Mo_2C nanocrystals on the edges and basal planes of MoS_2 (Fig. 4d). In addition, Zhu and co-workers successfully compounded the MoS_2 NSs with 1T-phase VS_2 nanoflowers (VS_2@MoS_2) using a two-step hydrothermal strategy for the first time.[99] The metallicity of VS_2 benefitted the charge-transfer efficiency, whereas the active edge of MoS_2 played a role in exposing active sites, and thus both of them synergistically enhanced the HER performance. Compared with VS_2 and MoS_2, VS_2@MoS_2 exhibited a low overpotential of 73 mV at -10 mA cm^{-2}, and a small Tafel slope of 55 mV dec^{-1}, which benefitted from the synergistic regulation of the composite material constituted using VS_2 and MoS_2. Furthermore, Jaramillo and co-workers synthesized core–shell nanowires, which were vertically oriented with a MoO_3 core and conformal MoS_2 shell, using low-temperature sulfidization.[100] Each component was designed to exhibit the best properties of core–shell architecture by precisely controlling the reaction conditions. The MoO_3 cores were around 20–50 nm and the MoS_2 shells were around 2–5 nm, and made the best of their respective advantages. The MoO_3 core supplied a high aspect ratio substrate and facilitated electron transport, while the MoS_2 shell provided catalytic activity and protected the catalyst from destruction in strong acids. Similarly, Chu and co-workers prepared a $WO_3 \cdot 2H_2O$/WS_2 hybrid catalyst by depositing a WS_2 film on CFP during *in situ* anodic oxidation (Fig. 4e).[101] Due to proton intercalation in $WO_3 \cdot 2H_2O$ followed by the transfer of hydrogen to WS_2, the synergistic effects between $WO_3 \cdot 2H_2O$ and WS_2 facilitate the kinetics of the HER on the planar defects and edges (Fig. 4f). The $WO_3 \cdot 2H_2O$/WS_2 catalyst exhibited a current density of -100 mA cm^{-2} at 152 mV overpotential and a Tafel slope of 54 mV dec^{-1}. Moreover, Liu and co-workers synthesized few-layered g-C_3N_4 NSs with vertically aligned MoS_2 loading (MoS_2/C_3N_4), which showed excellent PEC performance.[102] The Mo–N bonds connecting MoS_2 to C_3N_4 were responsible for receiving and conducting electrons, which determined the interfacial active sites as the regions of electron-accumulation. Therefore, the high catalytic activity was ascribed to the synergistic effect between layered g-C_3N_4 and MoS_2 and the excellent vertical structure. Moreover, on the basis of the complementary principle, Yang and co-workers reported a novel integrated quasi-planar structure of $MoSe_2$/Bi_2Se_3, which was synthesized using a hot injection in a colloidal system.[103] According to the UPS results, Bi_2Se_3 has a higher Fermi level and smaller work function than $MoSe_2$, which illustrates that Bi_2Se_3 possesses better electrical conductivity and could deliver electrons to $MoSe_2$ through close contact with the as-formed hetero-structured hybrids. Therefore, the integrated hetero-nanostructures between $MoSe_2$ NSs and Bi_2Se_3 NSs could synergistically boost supercapacitor performance and electrocatalytic water splitting. In addition, very active and stable hybrid electrocatalyst CoS_2 NSs, incorporated with WS_2 NSs (CoS_2@WS_2), were synthesized using a one-step sulfurization method for the first time.[104] The W-doped CoS_2 hybrid produced a fair amount of valence electrons, which could form more lattice defects, resulting in an increase in the accessible internal surface area and exposure of more active edge sites. The formation of nanointerfaces of Co–S–W between CoS_2 and WS_2 induced electron transfer through intermediate sulphur atoms, which were bonded to both metals. As a result, the good dispersion of WS_2 NPs, the enhanced electric conductivity, and the construction of Co–S–W nanointerfaces between CoS_2 and WS_2 effectively enhanced the HER activity.

As an earth-abundant electrocatalyst, MoS_2 exhibited excellent electrochemical performance towards the HER in an acidic solution, though it was retarded in an alkaline solution. Regarding this, it is worth emphasizing that layered double hydroxides (LDH), especially Ni-, Co-, Fe-based LDH, were able to effectively adsorb hydroxyl (OH) species and accelerate the dissociation.[105] Therefore, it is crucial to improve the reaction kinetics for the HER in alkaline electrolytes by compositing the MX_2-like catalysts with LDH. In order to develop high-activity MoS_2-based electrocatalysts suitable for unfavourable media, Yang and co-workers successfully designed and synthesized a synergistic hybrid catalyst system, which was made up of MoS_2 as an acceptor of H and LDH as an acceptor of OH, and which dramatically enhanced the HER activity in alkaline media.[41] The kinetic analysis of the activation free energies demonstrated that both MoS_2 and LDH accelerated the rate of water dissociation in the HER. The hybrid MoS_2/NiCo-LDH composite exhibited a low overpotential of 78 mV at a current of -10 mA cm^{-2} and a low Tafel slope of 76.6 mV dec^{-1} in a 1 M KOH solution. The successful introduction of LDH in MoS_2 further improved the MX_2 catalyst for use in pH-independent environments. Liang and co-workers reported a composite of nickel hydr(oxy)oxide NPs and 1T-phase MoS_2 NSs, which can significantly promote HER performance in neutral and alkaline electrolytes.[106] Impressively, they took advantage of both 1T-MoS_2 and $Ni_{2+\delta}O_\delta(OH)_{2-\delta}$ to play specific roles in different elementary reactions, which efficiently improved the performance of the overall HER. Because of the bifunctional mechanism applied in the composite catalysts, nickel hydr(oxy) oxide boosts the adsorption of water, and supplies protons by dissociation for subsequent process of MoS_2 for hydrogen generation, which enhanced the HER activity by driving an overpotential of 73 mV at a current density of -10 mA cm^{-2} in a 1 M KOH solution. In addition, Jiang and co-workers synthesized a nanostructured $Ni(OH)_2$/MoS_2, which synergized the interface between $Ni(OH)_2$ and MoS_2, and particularly boosted the efficiency of the HER in alkaline electrolytes.[107] The enhancement is mainly attributed to $Ni(OH)_2$ NPs, which promoted water dissociation. Then, the hydrogen intermediates recombined into molecular hydrogen on the surface of MoS_2, which could be an approach for collaborative optimization. Therefore, the synergistic effects between $Ni(OH)_2$ and MoS_2 resulted in the optimal energetics of hydrogen and hydroxyl species, which decreased the energy barriers of the initial water dissociation step and accelerated the subsequent generation of hydrogen. Based upon the synergy of multiple performances enhancing each other, the component integration built heterojunction structure of catalysts can improve the efficiency of water decomposition to obtain excellent catalytic performance. The architecture of heterostructures is highly advantageous for the disordered structure, and exposes abundant active hetero-interfaces from the synergistic

effect, setting up a highway of charge transport in channels, and accomplishing a dramatically improved performance for the electrocatalysis of overall water splitting.[108] Liu and co-workers reported that $Co(OH)_2$ NPs confined by MoS_2 NSs could accelerate the water dissociation and exhibit excellent catalytic activity in alkaline solutions, which significantly improved the HER performance.[109] In particular, the intercalation of $Co(OH)_2$ in MoS_2 NSs can prevent it from aggregating and, therefore, result in the expansion of the interlayer spacing in MoS_2 NSs, thus ensuring good durability.

As a typical HER electrocatalyst, MoS_2 possesses poor activity for the oxygen evolution reaction (OER). Jiang and co-workers synthesized a Co_3O_4@MoS_2 heterostructure, and used it as a highly efficient bifunctional electrocatalyst for the overall reaction of water splitting (Fig. 4g).[110] It is clear that structuring heterostructures could improve the sluggish kinetics to beneficially balance both the HER and OER activities, reduce the resistance of water dissociation and optimize hydrogen adsorption and desorption in alkaline media (Fig. 4h–i). Furthermore, Co_3O_4 NPs could enhance the adsorption of oxygen intermediates during the OER process. As a result, interface engineering applied to Co_3O_4@MoS_2 was an effective approach to establish an efficient bifunctional electrocatalyst, which had low overpotentials of 90 and 269 mV at 10 mA cm^{-2} in 1 M KOH for the HER and OER and corresponding Tafel slopes of 59.5 mV dec^{-1} and 58 mV dec^{-1}, respectively.

6. Conclusions

In this work, various approaches have been reviewed to enhance the catalytic activity and performance of MX_2-based materials (where M = Mo or W or V, and X = S or Se) towards the HER. Additionally, the latest discoveries in this field, which took place in the last three years, have also been highlighted. With the deepening of research, the catalytic performance of MX_2 and related compounds has made great progress. Although the HER performance of commercial Pt-based materials is still better than those of MX_2 materials, the experience gained through the study of MX_2 materials can guide the design of other families of HER catalysts in the future.

Conflicts of interest

All the authors have read the manuscript and have found no conflict of interest for its publication.

Acknowledgements

This work is supported by the National Natural Science Foundation of China (Grant No. 51372056, 51672057, and 51722205), National Science Fund for Distinguished Young Scholars (Grant No. 51525201), the Foundation for Innovative Research Groups of the National Natural Science Foundation of China (Grant No. 11421091), the International Science & Technology Cooperation Programme of China (Programme No. 2012DFR50020), the Fundamental Research Funds for the Central Universities (Grant No. HIT.BRETIV.201801), the Natural Science Foundation of Heilongjiang Province (Grant No. E2018032), and the Program for New Century Excellent Talents in University (NCET-13-0174).

Notes and references

1 J. A. Turner, *Science*, 2004, **305**, 972.
2 N. S. Lewis and D. G. Nocera, *Proc. Natl. Acad. Sci. U. S. A.*, 2006, **103**, 15729.
3 M. S. Faber and S. Jin, *Energy Environ. Sci.*, 2014, **7**, 3519–3542.
4 J. Greeley, T. F. Jaramillo, J. Bonde, I. Chorkendorff and J. K. Nørskov, *Nat. Mater.*, 2006, **5**, 909.
5 D. Merki and X. Hu, *Energy Environ. Sci.*, 2011, **4**, 3878.
6 T. Wang, H. Xie, M. Chen, A. D'Aloia, J. Cho, G. Wu and Q. Li, *Nano Energy*, 2017, **42**, 69–89.
7 Y. He and D. Wang, *Chem*, 2018, **4**, 405–408.
8 O. Khaselev and J. A. Turner, *Science*, 1998, **280**, 425.
9 M. A. Lukowski, A. S. Daniel, C. R. English, F. Meng, A. Forticaux, R. J. Hamers and S. Jin, *Energy Environ. Sci.*, 2014, **7**, 2608–2613.
10 J. D. Benck, T. R. Hellstern, J. Kibsgaard, P. Chakthranont and T. F. Jaramillo, *ACS Catal.*, 2014, **4**, 3957–3971.
11 A. B. Laursen, S. Kegnaes, S. Dahl and I. Chorkendorff, *Energy Environ. Sci.*, 2012, **5**, 5577–5591.
12 C. G. Morales-Guio and X. Hu, *Acc. Chem. Res.*, 2014, **47**, 2671–2681.
13 M. S. Faber, R. Dziedzic, M. A. Lukowski, N. S. Kaiser, Q. Ding and S. Jin, *J. Am. Chem. Soc.*, 2014, **136**, 10053–10061.
14 M. Chhowalla, H. S. Shin, G. Eda, L.-J. Li, K. P. Loh and H. Zhang, *Nat. Chem.*, 2013, **5**, 263.
15 F. H. Saadi, A. I. Carim, J. M. Velazquez, J. H. Baricuatro, C. C. L. McCrory, M. P. Soriaga and N. S. Lewis, *ACS Catal.*, 2014, **4**, 2866–2873.
16 J. D. Wiensch, J. John, J. M. Velazquez, D. A. Torelli, A. P. Pieterick, M. T. McDowell, K. Sun, X. Zhao, B. S. Brunschwig and N. S. Lewis, *ACS Energy Lett.*, 2017, **2**, 2234–2238.
17 H. Wang, D. Kong, P. Johanes, J. J. Cha, G. Zheng, K. Yan, N. Liu and Y. Cui, *Nano Lett.*, 2013, **13**, 3426–3433.
18 E. J. Popczun, J. R. McKone, C. G. Read, A. J. Biacchi, A. M. Wiltrout, N. S. Lewis and R. E. Schaak, *J. Am. Chem. Soc.*, 2013, **135**, 9267–9270.
19 J. F. Callejas, C. G. Read, C. W. Roske, N. S. Lewis and R. E. Schaak, *Chem. Mater.*, 2016, **28**, 6017–6044.
20 L.-A. Stern, L. Feng, F. Song and X. Hu, *Energy Environ. Sci.*, 2015, **8**, 2347–2351.
21 T. Jin, Q. Han, Y. Wang and L. Jiao, *Small*, 2017, **14**, 1703086.
22 P. C. K. Vesborg, B. Seger and I. Chorkendorff, *J. Phys. Chem. Lett.*, 2015, **6**, 951–957.
23 M. Zeng and Y. Li, *J. Mater. Chem. A*, 2015, **3**, 14942–14962.
24 Z. Chen, D. Higgins, A. Yu, L. Zhang and J. Zhang, *Energy Environ. Sci.*, 2011, **4**, 3167–3192.
25 C. G. Morales-Guio, L.-A. Stern and X. Hu, *Chem. Soc. Rev.*, 2014, **43**, 6555–6569.

26 Q. H. Wang, K. Kalantar-Zadeh, A. Kis, J. N. Coleman and M. S. Strano, *Nat. Nanotechnol.*, 2012, **7**, 699.
27 H. Vrubel, D. Merki and X. Hu, *Energy Environ. Sci.*, 2012, **5**, 6136–6144.
28 Y. Kim, H. K. Jackson David, D. Lee, M. Choi, T. W. Kim, S. Y. Jeong, H. J. Chae, W. Kim Hyun, N. Park, H. Chang, F. Kuech Thomas and J. Kim Hyung, *Adv. Funct. Mater.*, 2017, **27**, 1701825.
29 M. L. Tang, D. C. Grauer, B. Lassalle-Kaiser, V. K. Yachandra, L. Amirav, J. R. Long, J. Yano and A. P. Alivisatos, *Angew. Chem., Int. Ed.*, 2011, **50**, 10203–10207.
30 J. Xie, H. Zhang, S. Li, R. Wang, X. Sun, M. Zhou, J. Zhou, X. W. Lou and Y. Xie, *Adv. Mater.*, 2013, **25**, 5807–5813.
31 M. A. Lukowski, A. S. Daniel, F. Meng, A. Forticaux, L. Li and S. Jin, *J. Am. Chem. Soc.*, 2013, **135**, 10274–10277.
32 H. Li, C. Tsai, A. L. Koh, L. Cai, A. W. Contryman, A. H. Fragapane, J. Zhao, H. S. Han, H. C. Manoharan, F. Abild-Pedersen, J. K. Nørskov and X. Zheng, *Nat. Mater.*, 2015, **15**, 48.
33 H. I. Karunadasa, E. Montalvo, Y. Sun, M. Majda, J. R. Long and C. J. Chang, *Science*, 2012, **335**, 698.
34 Z. Lei, J. Zhan, L. Tang, Y. Zhang and Y. Wang, *Adv. Energy Mater.*, 2018, 1703482.
35 Q. Ding, F. Meng, C. R. English, M. Cabán-Acevedo, M. J. Shearer, D. Liang, A. S. Daniel, R. J. Hamers and S. Jin, *J. Am. Chem. Soc.*, 2014, **136**, 8504–8507.
36 Y. Yin, Y. Zhang, T. Gao, T. Yao, X. Zhang, J. Han, X. Wang, Z. Zhang, P. Xu, P. Zhang, X. Cao, B. Song and S. Jin, *Adv. Mater.*, 2017, **29**, 1700311.
37 M. Cabán-Acevedo, M. L. Stone, J. R. Schmidt, J. G. Thomas, Q. Ding, H.-C. Chang, M.-L. Tsai, J.-H. He and S. Jin, *Nat. Mater.*, 2015, **14**, 1245.
38 A. B. Laursen, P. C. K. Vesborg and I. Chorkendorff, *Chem. Commun.*, 2013, **49**, 4965–4967.
39 B. Song and S. Jin, *Joule*, 2017, **1**, 220–221.
40 L. Jiang, W. Fu, Y. Y. Birdja, M. T. M. Koper and G. F. Schneider, *Nat. Commun.*, 2018, **9**, 793.
41 J. Hu, C. Zhang, L. Jiang, H. Lin, Y. An, D. Zhou, M. K. H. Leung and S. Yang, *Joule*, 2017, **1**, 383–393.
42 Y. C. Chen, A. Y. Lu, P. Lu, X. Yang, C. M. Jiang, M. Mariano, B. Kaehr, O. Lin, A. Taylor, I. D. Sharp, L. J. Li, S. S. Chou and V. Tung, *Adv. Mater.*, 2017, **29**, 1703863.
43 T. F. Jaramillo, K. P. Jørgensen, J. Bonde, J. H. Nielsen, S. Horch and I. Chorkendorff, *Science*, 2007, **317**, 100.
44 D. Voiry, R. Fullon, J. Yang, C. de Carvalho Castro e Silva, R. Kappera, I. Bozkurt, D. Kaplan, M. J. Lagos, P. E. Batson, G. Gupta, A. D. Mohite, L. Dong, D. Er, V. B. Shenoy, T. Asefa and M. Chhowalla, *Nat. Mater.*, 2016, **15**, 1003.
45 Y. Yin, J. Han, Y. Zhang, X. Zhang, P. Xu, Q. Yuan, L. Samad, X. Wang, Y. Wang, Z. Zhang, P. Zhang, X. Cao, B. Song and S. Jin, *J. Am. Chem. Soc.*, 2016, **138**, 7965–7972.
46 C. Tan, Z. Luo, A. Chaturvedi, Y. Cai, Y. Du, Y. Gong, Y. Huang, Z. Lai, X. Zhang, L. Zheng, X. Qi, M. H. Goh, J. Wang, S. Han, X.-J. Wu, L. Gu, C. Kloc and H. Zhang, *Adv. Mater.*, 2018, **30**, 1705509.
47 X. Geng, Y. Jiao, Y. Han, A. Mukhopadhyay, L. Yang and H. Zhu, *Adv. Funct. Mater.*, 2017, **27**, 1702998.
48 K. Chang, X. Hai, H. Pang, H. Zhang, L. Shi, G. Liu, H. Liu, G. Zhao, M. Li and J. Ye, *Adv. Mater.*, 2016, **28**, 10033–10041.
49 J. Xie, J. Zhang, S. Li, F. Grote, X. Zhang, H. Zhang, R. Wang, Y. Lei, B. Pan and Y. Xie, *J. Am. Chem. Soc.*, 2013, **135**, 17881–17888.
50 K. D. Rasamani, F. Alimohammadi and Y. Sun, *Mater. Today*, 2017, **20**, 83–91.
51 M.-R. Gao, M. K. Y. Chan and Y. Sun, *Nat. Commun.*, 2015, **6**, 7493.
52 J. Zhang, C. Zhang, Z. Wang, J. Zhu, Z. Wen, X. Zhao, X. Zhang, J. Xu and Z. Lu, *Small*, 2017, 1703098.
53 L. Yin, X. Hai, K. Chang, F. Ichihara and J. Ye, *Small*, 2018, **14**, e1704153.
54 Y. Zhou, L. Silva Jose, M. Woods John, V. Pondick Joshua, Q. Feng, Z. Liang, W. Liu, L. Lin, B. Deng, B. Brena, F. Xia, H. Peng, Z. Liu, H. Wang, M. Araujo Carlos and J. Cha Judy, *Adv. Mater.*, 2018, **30**, 1706076.
55 Q. Tang and D.-e. Jiang, *ACS Catal.*, 2016, **6**, 4953–4961.
56 W. Bi, X. Li, R. You, M. Chen, R. Yuan, W. Huang, X. Wu, W. Chu, C. Wu and Y. Xie, *Adv. Mater.*, 2018, **30**, e1706617.
57 C. Zhang, S. Yang, J. Wu, M. Liu, S. Yazdi, M. Ren, J. Sha, J. Zhong, K. Nie, S. Jalilov Almaz, Z. Li, H. Li, I. Yakobson Boris, Q. Wu, E. Ringe, H. Xu, M. Ajayan Pulickel and M. Tour James, *Adv. Energy Mater.*, 2018, 1703487.
58 J. Deng, H. Li, J. Xiao, Y. Tu, D. Deng, H. Yang, H. Tian, J. Li, P. Ren and X. Bao, *Energy Environ. Sci.*, 2015, **8**, 1594–1601.
59 J. Deng, H. Li, S. Wang, D. Ding, M. Chen, C. Liu, Z. Tian, K. S. Novoselov, C. Ma, D. Deng and X. Bao, *Nat. Commun.*, 2017, **8**, 14430.
60 K. Tang, X. Wang, Q. Li and C. Yan, *Adv. Mater.*, 2017, **30**, 1704779.
61 K. Qi, S. Yu, Q. Wang, W. Zhang, J. Fan, W. Zheng and X. Cui, *J. Mater. Chem. A*, 2016, **4**, 4025–4031.
62 Y. Shi, Y. Zhou, D.-R. Yang, W.-X. Xu, C. Wang, F.-B. Wang, J.-J. Xu, X.-H. Xia and H.-Y. Chen, *J. Am. Chem. Soc.*, 2017, **139**, 15479–15485.
63 Y. Liu, X. Hua, C. Xiao, T. Zhou, P. Huang, Z. Guo, B. Pan and Y. Xie, *J. Am. Chem. Soc.*, 2016, **138**, 5087–5092.
64 X. Hai, W. Zhou, S. Wang, H. Pang, K. Chang, F. Ichihara and J. Ye, *Nano Energy*, 2017, **39**, 409–417.
65 D. Gao, B. Xia, C. Zhu, Y. Du, P. Xi, D. Xue, J. Ding and J. Wang, *J. Mater. Chem. A*, 2018, **6**, 510–515.
66 W. Xiao, P. Liu, J. Zhang, W. Song, Y. P. Feng, D. Gao and J. Ding, *Adv. Energy Mater.*, 2017, **7**, 1602086.
67 P. Liu, J. Zhu, J. Zhang, P. Xi, K. Tao, D. Gao and D. Xue, *ACS Energy Lett.*, 2017, **2**, 745–752.
68 X. Huang, M. Leng, W. Xiao, M. Li, J. Ding, T. L. Tan, W. S. V. Lee and J. Xue, *Adv. Funct. Mater.*, 2017, **27**, 1604943.
69 R. Ye, P. del Angel-Vicente, Y. Liu, M. J. Arellano-Jimenez, Z. Peng, T. Wang, Y. Li, B. I. Yakobson, S. H. Wei, M. J. Yacaman and J. M. Tour, *Adv. Mater.*, 2016, **28**, 1427–1432.
70 H. Wang, C. Tsai, D. Kong, K. Chan, F. Abild-Pedersen, J. K. Nørskov and Y. Cui, *Nano Res.*, 2015, **8**, 566–575.

71 T. Kosmala, H. Coy Diaz, H.-P. Komsa, Y. Ma, A. V. Krasheninnikov, M. Batzill and S. Agnoli, *Adv. Energy Mater.*, 2018, **8**, 1800031.
72 X. Huang, X. Qi, F. Boey and H. Zhang, *Chem. Soc. Rev.*, 2012, **41**, 666–686.
73 Z. Liu, Z. Zhao, Y. Wang, S. Dou, D. Yan, D. Liu, Z. Xia and S. Wang, *Adv. Mater.*, 2017, **29**, 1606207.
74 Y. Li, H. Li, K. Cao, T. Jin, X. Wang, H. Sun, J. Ning, Y. Wang and L. Jiao, *Energy Storage Materials*, 2018, **12**, 44–53.
75 R. Tan Sherman Jun, I. Abdelwahab, L. Chu, M. Poh Sock, Y. Liu, J. Lu, W. Chen and P. Loh Kian, *Adv. Mater.*, 2018, **30**, 1704619.
76 Y. Xu, W. Tu, B. Zhang, S. Yin, Y. Huang, M. Kraft and R. Xu, *Adv. Mater.*, 2017, **29**, 1605957.
77 X. Zhang, X. Yu, L. Zhang, F. Zhou, Y. Liang and R. Wang, *Adv. Funct. Mater.*, 2018, **28**, 1706523.
78 X. Wang, Y. Li, T. Jin, J. Meng, L. Jiao, M. Zhu and J. Chen, *Nano Lett.*, 2017, **17**, 7989–7994.
79 Y. Li, H. Wang, L. Xie, Y. Liang, G. Hong and H. Dai, *J. Am. Chem. Soc.*, 2011, **133**, 7296–7299.
80 X. Han, X. Tong, X. Liu, A. Chen, X. Wen, N. Yang and X.-Y. Guo, *ACS Catal.*, 2018, **8**, 1828–1836.
81 Y. Sun, F. Alimohammadi, D. Zhang and G. Guo, *Nano Lett.*, 2017, **17**, 1963–1969.
82 Y.-H. Choi, J. Lee, A. Parija, J. Cho, S. V. Verkhoturov, M. Al-Hashimi, L. Fang and S. Banerjee, *ACS Catal.*, 2016, **6**, 6246–6254.
83 H. Wang, Z. Lu, D. Kong, J. Sun, T. M. Hymel and Y. Cui, *ACS Nano*, 2014, **8**, 4940–4947.
84 H. Yu, X. Yu, Y. Chen, S. Zhang, P. Gao and C. Li, *Nanoscale*, 2015, **7**, 8731–8738.
85 F. Xia, H. Wang and Y. Jia, *Nat. Commun.*, 2014, **5**, 4458.
86 Z. Sofer, D. Sedmidubský, Š. Huber, J. Luxa, D. Bouša, C. Boothroyd and M. Pumera, *Angew. Chem.*, 2016, **128**, 3443–3447.
87 R. He, J. Hua, A. Zhang, C. Wang, J. Peng, W. Chen and J. Zeng, *Nano Lett.*, 2017, **17**, 4311–4316.
88 H. Liu, K. Hu, D. Yan, R. Chen, Y. Zou, H. Liu and S. Wang, *Adv. Mater.*, 2018, 1800295.
89 Y. H. Chang, C. T. Lin, T. Y. Chen, C. L. Hsu, Y. H. Lee, W. Zhang, K. H. Wei and L. J. Li, *Adv. Mater.*, 2013, **25**, 756–760.
90 H. Bi, I. W. Chen, T. Lin and F. Huang, *Adv. Mater.*, 2015, **27**, 5943–5949.
91 X. Zhang, F. Meng, S. Mao, Q. Ding, M. J. Shearer, M. S. Faber, J. Chen, R. J. Hamers and S. Jin, *Energy Environ. Sci.*, 2015, **8**, 862–868.
92 Q. Ding, J. Zhai, M. Caban-Acevedo, M. J. Shearer, L. Li, H. C. Chang, M. L. Tsai, D. Ma, X. Zhang, R. J. Hamers, J. H. He and S. Jin, *Adv. Mater.*, 2015, **27**, 6511–6518.
93 Q. Ding, B. Song, P. Xu and S. Jin, *Chem*, 2016, **1**, 699–726.
94 K. S. Novoselov, A. Mishchenko, A. Carvalho and A. H. Castro Neto, *Science*, 2016, **353**, aac9439.
95 Z. Cai, B. Liu, X. Zou and H.-M. Cheng, *Chem. Rev.*, 2018, **118**, 6091–6133.
96 M.-R. Gao, J.-X. Liang, Y.-R. Zheng, Y.-F. Xu, J. Jiang, Q. Gao, J. Li and S.-H. Yu, *Nat. Commun.*, 2015, **6**, 5982.
97 H. Zhu, J. Zhang, R. Yanzhang, M. Du, Q. Wang, G. Gao, J. Wu, G. Wu, M. Zhang, B. Liu, J. Yao and X. Zhang, *Adv. Mater.*, 2015, **27**, 4752–4759.
98 Z. Zhao, F. Qin, S. Kasiraju, L. Xie, M. K. Alam, S. Chen, D. Wang, Z. Ren, Z. Wang, L. C. Grabow and J. Bao, *ACS Catal.*, 2017, **7**, 7312–7318.
99 X. Chen, K. Yu, Y. Shen, Y. Feng and Z. Zhu, *ACS Appl. Mater. Interfaces*, 2017, **9**, 42139–42148.
100 Z. Chen, D. Cummins, B. N. Reinecke, E. Clark, M. K. Sunkara and T. F. Jaramillo, *Nano Lett.*, 2011, **11**, 4168–4175.
101 L. Yang, X. Zhu, S. Xiong, X. Wu, Y. Shan and P. K. Chu, *ACS Appl. Mater. Interfaces*, 2016, **8**, 13966–13972.
102 H. Bian, Y. Ji, J. Yan, P. Li, L. Li, Y. Li and S. Liu, *Small*, 2017, **14**, 1703003.
103 J. Yang, C. Wang, H. Ju, Y. Sun, S. Xing, J. Zhu and Q. Yang, *Adv. Funct. Mater.*, 2017, **27**, 1703864.
104 X. Zhou, X. Yang, H. Li, M. N. Hedhili, K.-W. Huang, L.-J. Li and W. Zhang, *J. Mater. Chem. A*, 2017, **5**, 15552–15558.
105 H. Liang, F. Meng, M. Cabán-Acevedo, L. Li, A. Forticaux, L. Xiu, Z. Wang and S. Jin, *Nano Lett.*, 2015, **15**, 1421–1427.
106 X. Zhang and Y. Liang, *Adv. Sci.*, 2018, **5**, 1700644.
107 B. Zhang, J. Liu, J. Wang, Y. Ruan, X. Ji, K. Xu, C. Chen, H. Wan, L. Miao and J. Jiang, *Nano Energy*, 2017, **37**, 74–80.
108 J. Hou, B. Zhang, Z. Li, S. Cao, Y. Sun, Y. Wu, Z. Gao and L. Sun, *ACS Catal.*, 2018, **8**, 4612–4621.
109 Y. Luo, X. Li, X. Cai, X. Zou, F. Kang, H. M. Cheng and B. Liu, *ACS Nano*, 2018, **12**, 4565–4573.
110 J. Liu, J. Wang, B. Zhang, Y. Ruan, H. Wan, X. Ji, K. Xu, D. Zha, L. Miao and J. Jiang, *J. Mater. Chem. A*, 2018, **6**, 2067–2072.

